Monolithic Carbide-Derived Carbon Films for Micro-Supercapacitors

John Chmiola, Céline Largeot, Pierre-Louis Taberna, Patrice Simon, Yury Gogotsi

Monolithic Carbide-Derived Carbon Films for Micro-Supercapacitors

John Chmiola,[1]* Celine Largeot,[2] Pierre-Louis Taberna,[2] Patrice Simon,[2] Yury Gogotsi[1]†

Microbatteries with dimensions of tens to hundreds of micrometers that are produced by common microfabrication techniques are poised to provide integration of power sources onto electronic devices, but they still suffer from poor cycle lifetime, as well as power and temperature range of operation issues that are alleviated with the use of supercapacitors. There have been a few reports on thin-film and other micro-supercapacitors, but they are either too thin to provide sufficient energy or the technology is not scalable. By etching supercapacitor electrodes into conductive titanium carbide substrates, we demonstrate that monolithic carbon films lead to a volumetric capacity exceeding that of micro- and macroscale supercapacitors reported thus far, by a factor of 2. This study also provides the framework for integration of high-performance micro-supercapacitors onto a variety of devices.

Microbatteries with the capability to be fabricated with length scales controlled in the micrometer range improve performance over their larger cousins by decreasing diffusion lengths, increasing the fraction of electroactive materials and making use of precise fabrication protocols. The prospect of integrating microbatteries as discrete power sources with the micro-electromechanical systems (MEMS), the devices they power, and the capacity for autonomous recharging represents a conceptual leap forward over existing methods for powering devices. This could potentially increase the density of devices allowing improved functionality, reduced complexity, and enhanced redundancy by removing intricate interconnects to bulk-sized batteries. Currently, advanced rechargeable microbatteries that use thin-film technologies are commercially available (*1*), but they suffer from many of the limitations of their larger counterparts, namely limited cycle life, abrupt failure, poor low-temperature kinetics, and safety concerns associated with using lithium (*2*). Even three-dimensional (3D) batteries (*1*), which are expected to overcome power limitations by further shortening electrolyte path lengths, cannot avoid fast failure because of the inevitable self-discharge caused by electron tunneling through marginally conductive thin dielectric coatings (solid electrolytes) and repeated recharging cycles. Electrochemical capacitors (ECs), also called ultracapacitors or supercapacitors, can solve these lifetime and power issues and provide a bridge between devices operating with short charge-discharge times (<0.1 s) and longer discharge times (>0.1 hours) under and over which dielectric or electrolytic capacitors and batteries, respectively, find their niche (*3*). However, compared to lithium-ion batteries, very little work has been done to integrate ECs on a chip or to produce thin- and thick-film ECs in general.

The power density and cycle time of ECs enable them to improve the efficiency of a battery when the two are used together (*4*). ECs can harvest the excess kinetic energy, such as in the braking of a motor vehicle or the vibrations of a moving object. ECs store energy through reversible ion adsorption at the surface of high–specific surface area carbons at the carbon-electrolyte interface, in a so-called double-layer (*3*), whereas batteries store electrical energy in chemical bonds in a bulk material (*5*, *6*). ECs do not require slow charge or discharge to satisfy relatively sluggish electrochemical charge-transfer kinetics that maintain the thermodynamic steady state in batteries. Additionally, because only physical motion of charge carriers dictates the charge stored (*7*), they can handle currents that are larger by several orders of magnitude (*8*). Moreover, because EC electrostatics avoids battery and fuel-cell chemical kinetics, EC efficiency and reversibility exceed 90%, even at very high discharge rates (*4*). In combination with a practically infinite cycle life, ECs seem ideal for capturing and storing energy from renewable resources and for on-chip operation.

There have been notable advances in the micro-supercapacitor field, which were mostly focused on increasing micro-supercapacitor energy density by using different active materials (*9*) and designs, such as carbon nanotubes (CNTs) (*10*, *11*), activated carbons (*12*), polymers (*13*),

[1]Department of Materials Science and Engineering and A. J. Drexel Nanotechnology Institute, Drexel University, Philadelphia, PA 19104, USA. [2]Université Paul Sabatier de Toulouse, Inter-University Research and Engineering Center on Materials (CIRIMAT), UMR-CNRS 5085, 31062 Toulouse Cedex 4, France.

*Present address: Environmental Energy Technologies Division, Lawrence Berkeley National Laboratory, Berkeley, CA 94720, USA.

†To whom correspondence should be addressed. E-mail: gogotsi@drexel.edu

and metal oxides (*13*, *14*). CNT films were used in 2D thin-film micro-supercapacitors with several square centimeter footprints; the "micro-" prefix referring here to the film thickness (about 10 μm thick) (*10*, *15*). The films gave respectable gravimetric and volumetric capacitance, but the functional capacitance per unit area of device was low (*10*). Activated carbon powders have a better performance in terms of energy per unit area (*12*), but they need to be processed into films before use, and this limits their interest for microdevice fabrication. Conducting polymers have shown fairly good performance (*13*, *16*), but are not yet compatible with standard microfabrication protocols. Oxide-based thin-film ECs have shown high performance, approaching the theoretical limit for capacitance (for example, 1000 F/g for MnO_2) (*17*, *18*). However, the poor electrical conductivity and high impedances associated with surface intercalation redox reactions of these oxides have limited practical film thicknesses to a few microns. Nanotubes have been added to the films to increase the electrical conductivity, but the complexity of manufacturing limits practical applications of such composite electrodes.

Carbide-derived carbon (CDC) is a class of carbon materials produced by selectively etching metals from metal carbides using chlorine at elevated temperatures in a process that is similar to current dry-etching techniques for MEMS and microchip fabrication. CDC has been shown to have excellent performance as the active material in traditionally processed ECs (*19*), because it can have its microstructure precisely tuned by tailoring the synthesis conditions for a particular electrolyte (*20*). In the realm of microfabricated supercapacitors, CDC is attractive for two reasons: First, the precursor carbides are conductive and can be deposited in uniform thin and thick films by well-known chemical and physical vapor deposition (CVD and PVD, respectively) techniques (*21*). Then the chlorination process can be performed at temperatures at least as low as 200°C (*22*), and the resulting coatings are well-adhered with an atomically perfect interface (*23*), which minimizes device impedance. This technology can be used to produce the microfabricated ECs on the same chip as the integrated circuits, which they are powering, as schematically shown in Fig. 1. Chlorine-containing plasma etching of materials in semiconductor manufacturing is a well-established technique and is similar to the chlorination procedure in CDC manufacturing. Continuous porous carbon films cannot be produced by conventional CVD, PVD, or other techniques, and the high-temperature activation needed to produce the microstructures necessary for supercapacitor performance in CVD carbons would destroy the devices they were intended to power.

As a first step toward integrated energy-storage devices, thin CDC films were produced on bulk TiC ceramic plates. The electrochemical behavior was studied in two common EC electrolytes, aqueous sulfuric acid and tetraethylammonium tetrafluoroborate ($TEABF_4$) in acetonitrile.

This approach also allows for the study of carbons without interparticle porosity, which could potentially decrease the diffusion length and increase the number of ions available for charge storage in a unit volume. It could also aid in generating an understanding of the diffusion limi-

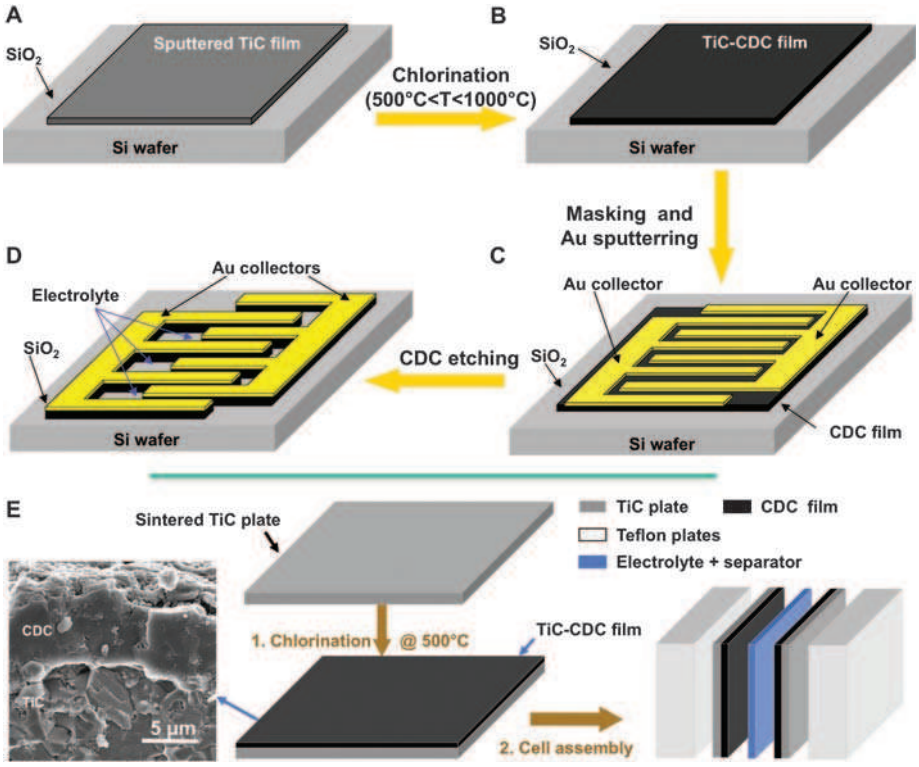

Fig. 1. (**A** to **D**) Schematic of the fabrication of a micro-supercapacitor integrated onto a silicon chip based on the bulk CDC film process. Standard photolithography techniques can be used for fabricating CDC capacitor electrodes (oxidative etching in oxygen plasma) and deposition of gold current collectors. (**E**) CDC synthesis and electrochemical test cell preparation schematic. Ti is extracted from TiC as $TiCl_4$, forming a porous carbon film. Two TiC plates with the same CDC coating thickness ranging from 1 to 200 μm are placed face to face and separated by a polymer fabric soaked with the electrolyte. SEM micrograph shows a representative image of a CDC/TiC interface, with a good film adhesion and a glassy film fracture surface typical of amorphous carbon.

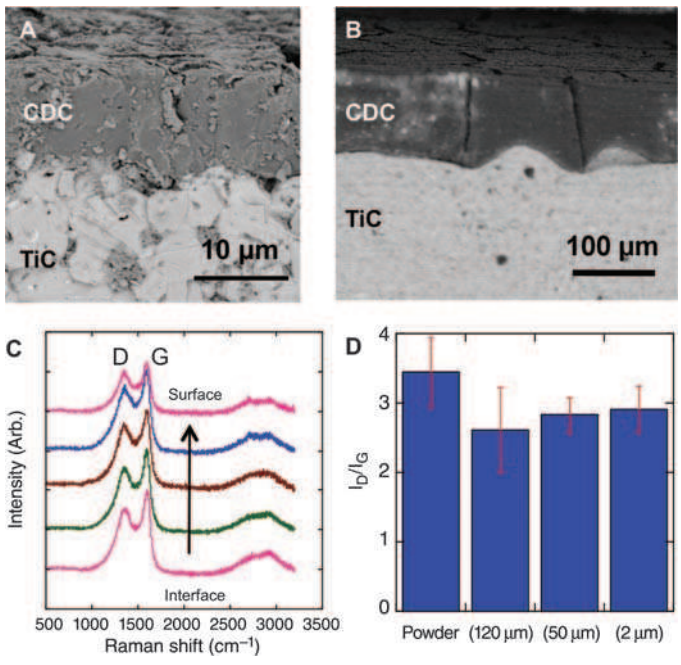

Fig. 2. CDC films on TiC. (**A**) Backscattered electron image showing a uniform carbon film and a strong TiC/CDC interface on a sample chlorinated for about 1 min. (**B**) Backscattered electron image showing a thick carbon film (5-min chlorination, ~100-μm film) with good adhesion, in spite of some microcracking. (**C**) Raman spectra show no major change in the structure of the film from the carbon-TiC interface to the surface of a ~50-μm film. Arb, arbitrary units. (**D**) Comparison of intensity ratios of D and G bands of graphitic carbon shows that there is little difference in the carbon structure of the films with the thickness ranging from 2 to 120 μm.

tations that may exist in thicker films when transport porosity in the form of interstitial voids between carbon particles in traditionally processed electrodes is removed. Likewise, as the electrolyte density is larger than the bulk density of activated carbon, monolithic porous films without interparticle porosity should show improved overall performance simply due to elimination of excess electrolytes located in macropores.

Sintered TiC ceramic plates (Angstrom Sciences, Duquesne, PA, purity > 99.5%, density = 4.93 g/cm^3) were cut to size and polished to be as thin as practically feasible (~300 μm) to minimize resistance before being chlorinated on one face for times ranging from 15 s to 5 min, which led to coatings from ~2 to ~200 μm. Scanning electron microscopy (SEM) images of ~5-μm (Fig. 1E), ~10-μm (Fig. 2A), and ~100-μm (Fig. 2B) films show a fairly uniform thickness and good adherence to the underlying TiC; similar results were obtained with all the samples. The film thickness for each sample was measured with the use of SEM. 500°C was chosen as the chlorination temperature because, at lower synthesis temperatures, the pore size has been shown to be too small for effective storage of tetraethylammonium cations (*24*), and at synthesis temperatures higher than this, the chlorination kinetics are too fast to have good control over coating thickness.

SEM micrographs of the film surface (Fig. 2, A and B) show some microcracking due to tensile stresses that develop in the film after Ti removal. The amount of microcracking increases with increasing coating thickness, but the cracks stay confined in the surface layer. The plates retain their shape and do not fall apart, even after complete transformation to carbon, and the microcracking that has already occurred did not lead to CDC film delamination from the TiC substrate. Raman spectroscopy of the coating surface for three different coating thicknesses (Fig. 2C) shows that the intensity ratio of disorder-induced (D) and graphite (G) bands of carbon (I_D/I_G) slightly decreases with increasing coating thickness, indicating a possible increase in microstructural ordering for thicker films at the surface. This is in line with SEM observations showing increasing relaxation of stresses at the surface. A longer time at elevated temperatures during the synthesis for thicker films leads to somewhat higher levels of ordering.

Raman microspectroscopy of a ~50-μm film (Fig. 2C) showed a fairly uniform I_D/I_G ratio throughout the coating thickness. At the film surface, there seems to be a slightly larger amount of ordering, but in general, the coatings are all of very similar microstructure. This increased ordering at the surface is probably related to the microcracking. The fact that Raman spectra (collected from the surface of coatings with different thickness and throughout the thickness of a 50-μm coating) are fairly consistent leads us to believe that the carbon is of very similar microstructure and porosity. The gas sorption isotherms of bulk CDC plates were similar to those of powders and, although precise sorption measurements on thin CDC films were impossible, we anticipate that the pore size of the samples was very close to 0.7 nm, as measured on TiC-CDC powders synthesized at 500°C (*24*).

Electrochemical measurements of CDC films were carried out in a three-electrode configuration with a large overcapacitive activated carbon counter-electrode in both 1 M $TEABF_4$ and 1 M H_2SO_4, as well as two-electrode cells with symmetric bulk CDC film electrodes (see the supporting online material for details). Three-electrode cells were used to evaluate Faradaic processes that may be present and the available potential window, and two-electrode cells were constructed to simulate actual device behavior. These electrolytes were chosen because they represent the most widely studied aqueous and organic electrolytes and are the most commercially used. Cyclic voltammograms (CVs) for 50-μm traditionally processed 500°C TiC-CDC powder electrodes are also included for direct comparison. Both CVs of CDC films show good non-Faradaic response, with voltage windows similar to powder electrodes (Fig. 3). If there were a substantial amount of impurities due to chlorine and chlorides being trapped in the film, there would be Faradaic currents, especially at the extents of cycling. In H_2SO_4 (Fig. 3B), there are minor current peaks at both of the switching potentials, the origin of which needs to be studied further; the peaks, however, decrease with cycling. The shape of the CV is different for the forward sweep and backward sweep, which shows the importance of pore accessibility, desolvation, and effective ion sizes (*24*, *25*). Recent studies have shown that the TEA^+ cation may have difficulties entering very small pores because of its larger size relative to BF_4^-, hence the slower saturation for the negative scan and an asymmetric behavior (*26*, *27*). Accordingly, the tetraethylammonium cation adsorption drives the electrochemical behavior at high cell voltage.

Volumetric capacitance was calculated for each of the different film thicknesses (Fig. 4). For both $TEABF_4$ and H_2SO_4, the volumetric capacitance decreases with increasing coating thickness. This is especially pronounced in the organic electrolyte, where there is a huge increase in volumetric capacitance as the film thickness decreases from 200 to ~2 μm. For a CDC film of ~50 μm in $TEABF_4$, the volumetric capacitance (~60 F/cm^3) is similar to what was observed in a ~300-μm traditionally processed electrode from carbon powders (~50 F/cm^3) (*25*). Likewise, in 1M H_2SO_4 electrolyte, for films thicker than ~100 μm, the

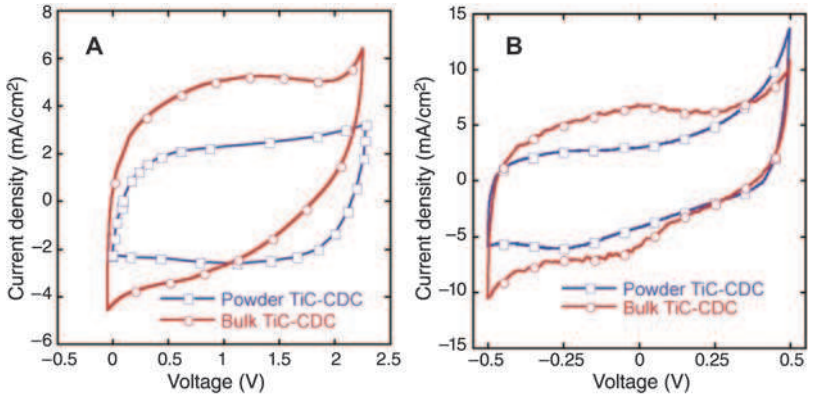

Fig. 3. Cyclic voltammetry data for CDC films in two-electrode cells. (**A**) A ~50-μm film and a ~50-μm traditional powder electrode in $TEABF_4$. (**B**) A ~50-μm film and a ~50-μm traditional powder electrode in H_2SO_4. Monolithic CDC shows a larger capacitance compared with powder electrodes even in fairly thick films.

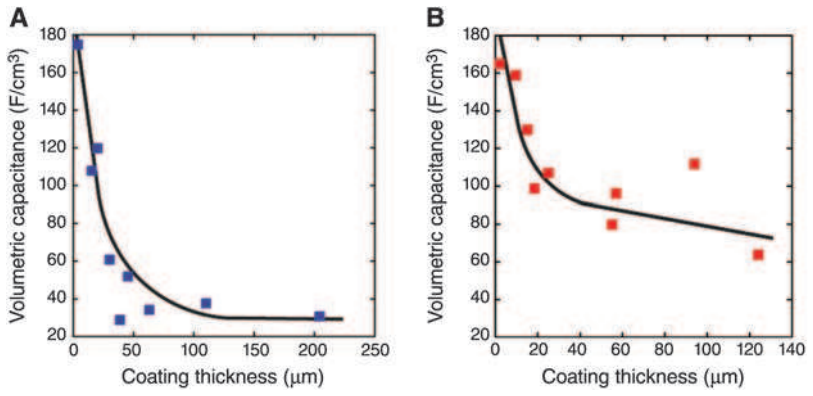

volumetric capacitance is similar to what was measured on a ~300-μm-thick traditionally processed electrode (~80 F/cm^3).

As the coating thickness decreases to ~2 μm, the volumetric capacitance increases to nearly 180 F/cm^3 in $TEABF_4$ electrolyte and ~160 F/cm^3 in 1M H_2SO_4. The spacing between cracks is larger than the film thickness (Fig. 3B); thus, electrolyte transport is controlled by the transport from bulk electrolyte to the current collector through the entire film thickness, making crack influence on capacitance marginal at best. Also, the crack volume in comparison with the pore volume of the CDC layer (>50%) does not lead to a substantial increase in electrolyte volume or electrode surface area (<1%). Simply removing ~50% of empty volume between particles in traditional electrodes would provide volumetric capacitance numbers of ~100 F/cm^3 in organic electrolyte and ~160 F/cm^3 in sulfuric acid electrolyte; it is believed that this is the major reason for the thin-film results. The extremely intimate contact between the underlying current collector and CDC film would also facilitate good electron transfer into the film, limiting the voltage drop through this interface and resulting in higher charge compensation in the double-layer, which could explain capacitance values above what is expected based solely on sphere-packing assumptions. The decrease in capacitance with thicker films is most likely due to microstructural rearrangement from surface stresses relaxing, which results in porosity collapse and perturbation of the interconnected structure that facilitates electron conduction. The effects of electrolyte starvation with thicker films coupled to structure collapse may also play a role in the drop in capacitance values [as previously shown by Zheng *et al*. (*28*)], with thicker films requiring a larger number of ions to migrate from the bulk electrolyte into the pore structure.

Although we observed microcracking in the TiC-CDC films in this study, it has previously been shown that dense coatings can be made to 200-μm thickness for SiC-CDC films (*29*). Earlier work chlorinating sputtered amorphous TiC, which is the simplest method for patterning carbide substrates for micro-supercapacitors on devices, has shown that TiC-CDC can also be produced crack-free, at least in the form of 0.5-μm films (*21*). Therefore, in terms of extrapolating these results to realizable micro-supercapacitors, we expect that what may be viewed as technological hurdles should, in fact, lead to better-functioning devices.

References and Notes

1. J. W. Long, B. Dunn, D. R. Rolison, H. S. White, *Chem. Rev.* **104**, 4463 (2004).
2. M. Armand, J. M. Tarascon, *Nature* **451**, 652 (2008).
3. P. Simon, Y. Gogotsi, *Nat. Mater.* **7**, 845 (2008).
4. J. Miller, A. F. Burke, *Electrochem. Soc. Interface* **17 (Spring)**, 53 (2008).
5. R. J. Brodd *et al*., *J. Electrochem. Soc.* **151**, K1 (2004).
6. D. Linden, Ed., *Handbook of Batteries* (McGraw-Hill, New York, ed. 2, 2001).
7. A. Tanimura, A. Kovalenko, F. Hirata, *Chem. Phys. Lett.* **378**, 638 (2003).
8. B. W. Ricketts, C. Ton-That, *J. Power Sources* **89**, 64 (2000).
9. A. S. Aricò, P. Bruce, B. Scrosati, J.-M. Tarascon, W. van Schalkwijk, *Nat. Mater.* **4**, 366 (2005).
10. V. L. Pushparaj *et al*., *Proc. Natl. Acad. Sci. U.S.A.* **104**, 13574 (2007).
11. S. W. Lee, B.-S. Kim, S. Chen, Y. Shao-Horn, P. T. Hammond, *J. Am. Chem. Soc.* **131**, 671 (2009).
12. D. Pech *et al*., *J. Power Sources* **195**, 1266 (2010).
13. W. Sun, X. Y. Chen, *Microelectron. Eng.* **86**, 1307 (2009).
14. J. Wang, J. Polleux, J. Lim, B. Dunn, *J. Phys. Chem. C* **111**, 14925 (2007).
15. M. Kaempgen, C. K. Chan, J. Ma, Y. Cui, G. Gruner, *Nano Lett.* **9**, 1872 (2009).
16. K. Naoi, M. Morita, *Electrochem. Soc. Interface* **17** (Spring), 44 (2008).
17. H. J. Ahn, W. B. Kim, T. Y. Seong, *Electrochem. Commun.* **10**, 1284 (2008).
18. M. J. Lee *et al*., *J. Electroceram.* **17**, 639 (2006).
19. J. Leis, M. Arulepp, A. Kuura, M. Latt, E. Lust, *Carbon* **44**, 2122 (2006).
20. A. Jänes, E. Lust, *J. Electrochem. Soc.* **153**, A113 (2006).
21. E. N. Hoffman, G. Yushin, B. G. Wendler, M. W. Barsoum, Y. Gogotsi, *Mater. Chem. Phys.* **112**, 587 (2008).
22. R. K. Dash, G. Yushin, Y. Gogotsi, *Microporous Mesoporous Mater.* **86**, 50 (2005).
23. Z. G. Cambaz, G. N. Yushin, Y. Gogotsi, K. L. Vyshnyakova, L. N. Pereselentseva, *J. Am. Ceram. Soc.* **89**, 509 (2006).
24. J. Chmiola, C. Largeot, P. L. Taberna, P. Simon, Y. Gogotsi, *Angew. Chem. Int. Ed.* **47**, 3392 (2008).
25. J. Chmiola *et al*., *Science* **313**, 1760 (2006); published online 17 August 2006 (10.1126/science.1132195).
26. R. Lin *et al*., *J. Electrochem. Soc.* **156**, A7 (2009).
27. R. Mysyk, E. Raymundo-Pinero, F. Beguin, *Electrochem. Commun.* **11**, 554 (2009).
28. J. P. Zheng, J. Huang, T. R. Jow, *J. Electrochem. Soc.* **144**, 2417 (1997).
29. D. A. Ersoy, M. J. McNallan, Y. Gogotsi, *Mater. Res. Innovations* **5**, 55 (2001).

30. Electron microscopy and Raman spectroscopy analyses were conducted with the use of instruments in the Centralized Research Facility of the College of Engineering, Drexel University and Université Paul Sabatier de Toulouse. J.C. was supported by Integrative Graduate Education and Research Traineeship (IGERT) and Graduate Research fellowships from the NSF, C.L. was supported by Délégation Générale pour l'Armement, and Y.G. was supported by the U.S. Department of Energy, Office of Basic Energy Sciences, Division of Materials Sciences and Engineering under award ER46473. Collaboration between the participating universities was supported by a Partnership University Fund grant. Y.G. is also Founder and Chief Science Officer, Y-Carbon. The authors also have a related patent application no. 61/025058.